High dynamic range imaging in space: overview and wavefront control

Amir Give'on, Stuart B. Shaklan, Joseph J. Green

Amir Give'on, Stuart B. Shaklan, Joseph J. Green, "High dynamic range imaging in space: overview and wavefront control," Proc. SPIE 6288, Current Developments in Lens Design and Optical Engineering VII, 62880A (31 August 2006); doi: 10.1117/12.682057

SPIE.

Event: SPIE Optics + Photonics, 2006, San Diego, California, United States

High-Dynamic Range Imaging in Space: Overview and Wavefront Control

Amir Give'on[a], Stuart B. Shaklan[b] and Joseph J. Green[b]

[a]California Institute of Technology, Pasadena, CA;

[b]Jet Propulsion Laboratory, Pasadena, CA

ABSTRACT

NASA is endeavoring to launch missions capable of detecting Earth-like planets around neighboring stars. In visible wavelengths, this requires better than 10^{-10} suppression of scattered light as close as 50 milli-arcsec to the stellar image. This extraordinary requirement is within reach but it requires broad-band wave front control to sub-Angstrom levels. We describe several high dynamic range imaging solutions, describe the various factors that contribute to the scattered light level and introduce a novel closed-loop broad-band correction system, suitable for the Shaped Pupil Coronagraph and the Lyot Coronagraph.

Keywords: Adaptive optics, high contrast imaging

1. INTRODUCTION

The Terrestrial Planet Finder Coronagraph[1] (TPF-C) is a planned 8m × 3.5m space-based observatory capable of directly detecting and characterizing starlight reflected from terrestrial planets orbiting nearby stars. The observatory is required to find earth-like planets in the so-called "habitable zone," where liquid water can exist, covering roughly 0.7 - 1.5 AU from a solar-type star. These planets appear close to their star and very faint. The goal of TPF is to survey the habitable zone of the nearest ∼150 F, G, and K stars (within 20 pc away from Earth), for the existence of terrestrial planets. TPF is to be designed to be able to determine various orbital parameters and even mass. TPF will also carry out spectroscopy (with low and medium resolution) for signatures of biomarkers on the discovered planets.[3–5] Figure 1 shows the schematic of the TPF-C Elements.

The critical challenge any Earth-like planet imaging system must overcome is the high contrast between the light coming from the star and the light reflected back from the planet.[6,7] The contrast between the star and an Earth-like planet is on the order of one 10 billionth (10^{-10}) when operating in the visible light region of the spectrum. That is, 10 billion times more photons, on average, would arrive at a distant observatory from the Sun than from the Earth.

Standard telescopes, with a circular aperture of diameter D, have a limited resolution due to diffraction effects. The first "diffraction null" for these optical systems occurs at roughly 1.22 λ/D (where λ is the wavelength). In order to resolve the planets 60 milliarcsec from their host stars, assuming observations at 0.6 micron and a best high contrast system angular resolution of 4 λ/D, the diameter of the primary mirror of the observatory must be roughly 8 meters. It is not necessary to make the entrance pupil circular.[8] Using an elliptical aperture allows for sufficient area (photon collection) with the needed resolution in the direction of the long axis of the elliptical aperture and a Point Spread Function (PSF) that satisfies the high contrast system requirements.

In this paper we will describe several proposed high-contrast techniques and present their advantages and disadvantages. The greatest challenge facing any high contrast imaging system is wavefront control, namely, amplitude and phase compensation to sub-Angstrom levels. We will introduce the "Peak-a-boo" correction algorithm - a closed loop correction algorithm that uses a pinhole in a pupil plane in order to reconstruct the real and imaginary parts of the electric field in the image plane.

Current Developments in Lens Design and Optical Engineering VII, edited by Pantazis Z. Mouroulis, Warren J. Smith, R. Barry Johnson, Proc. of SPIE Vol. 6288, 62880A, (2006) · 0277-786X/06/$15 · doi: 10.1117/12.682057

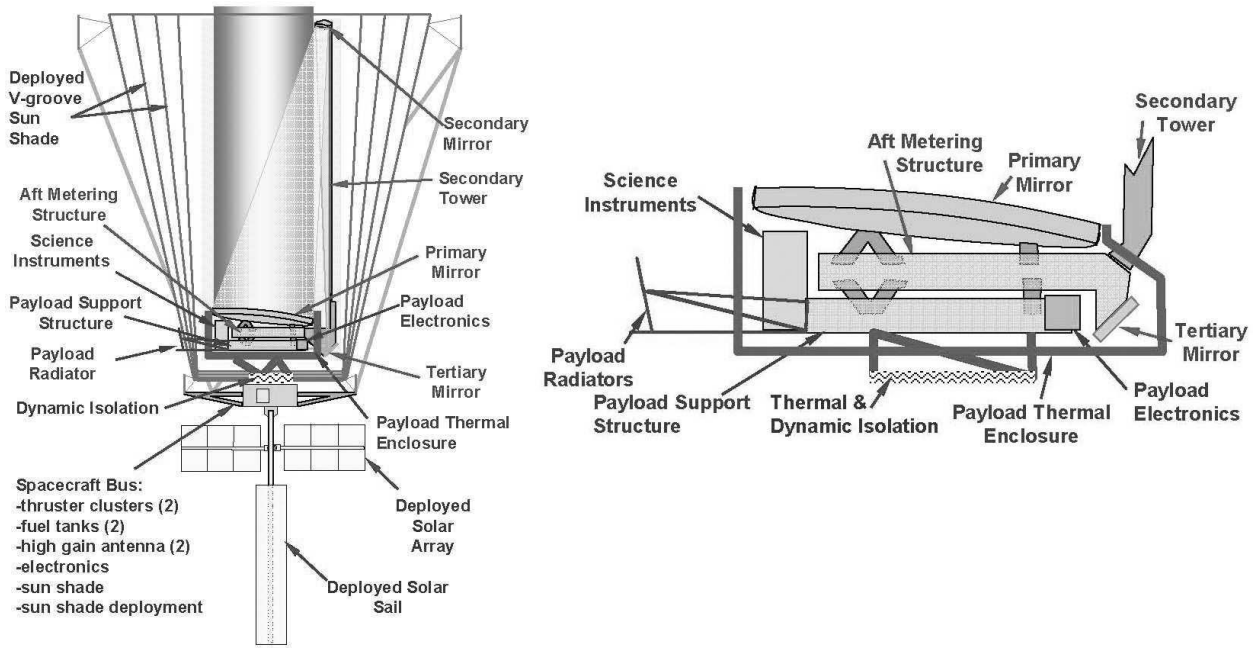

Figure 1. The schematic of the TPF-C Elements

2. PROPOSED SOLUTIONS

Several coronagraph designs have been proposed as a solution to this formidable task of imaging Earth-like planets. The traditional coronagraph approach utilizes an image plane occulter (typically Gaussian) followed by a Lyot stop at a reimaged pupil.[9] A newer proposed coronagraph design utilizes bandlimited masks.[10] While the basic approach is the same, replacing the Gaussian field stop with a bandlimited function dramatically improves contrast and increases throughput. One of the advantages of this approach is its ability to search all azimuths at once. Its main disadvantages are the difficulty in manufacturing the field stops with the needed precision, the sensitivity to pointing error, and poor broadband performance. We determined that polarization and wavelength dependence prevent us from using binary masks.

The optical vortex coronagraph (OVC)[12] is another form of Lyot coronagraph. It is in a sense a generalization of the four-quadrant coronagraph.[13] Like the 4-quadrant mask, the OVC is a phase-only filter that cancels the light from an on-axis source and scatters it outside the geometrical pupil. It has substantially higher throughput and higher image plane resolution than other Lyot coronagraphs because the Lyot stop is then the same size as the pupil and the OVC mask itself is non-absorptive. The OVC has an important advantage over the 4-quadrant solution that produces a superior rejection of starlight; the dark hole at the center of the OVC can be of higher order (it has steep walls), a necessary condition to reduce scattered light from the finite-size stars. The higher-order also reduces aberration sensitivity[14,16] which makes the mask attractive for use at small inner working angles (e.g. the 2nd or 3rd Airy ring). The masks are made using e-beam fabrication in optical polymers[14] and are intrinsically dispersive. Schwartzlander et al[15] have described a simple achromatization approach. The TPF-C project is studying the performance of the mask and hope to implement it in the High Contrast Imaging Testbed[17] in 2007.

The Phase-Induced Amplitude Apodization Coronagraph (PIAAC)[19] is another proposed solution to the high contrast imaging problem. The PIAAC uses a lossless beam apodization, performed by aspheric mirrors, to produce a high contrast PSF. This concept theoretically offers a unique combination of high throughput, high angular resolution, small inner working angle, low chromaticity and low sensitivity to pointing errors or angular star diameter. A new hybrid configuration adds appodizers.[20] These modifications control diffraction effects, increase bandwidth, and relax tolerancing at the outer edge of the remapping optic. The PIAAC is under

testing at the University of Hawaii, where they have taken deliver of the first high-quality unit. We do not yet understand how the system will behave with a wavefront control system.

Another proposed solution is the Shaped Pupil Coronagraph (SPC).[21] The SPC is a telescopic system in which one of the conjugate planes to the plane of the primary mirror is apodized. However, rather than smoothly apodizing this plane,[22,23] the *shape* of the aperture is optimized. Specific shapes can be found that result in an image with the needed contrast for detection of Earth like plants.[24]

The advantages of this method are that it can work without a glass substrate, so no multiple reflections occur (surface quality and homogeneity are inconsequential); being in the pupil plane, mask dimensions are much greater than the wavelength so polarization and bandwidth effects are small; and lastly, manufacturing of such masks with the specifications for TPF is within reach with current technology. The potential limitation of the SPC is that it provides discovery only over limited azimuths, requiring a rotation of the observatory, reduced throughput compared to phase-only schemes, and broader point spread functions resulting in larger zodiacal light contributions. However, in order to perform characterization of a planet, where the planet position is known, very narrow discovery spaces can be used resulting in substantial improvements in integration times.

3. SYSTEM ABERRATIONS

Unfortunately, all imaging systems are imperfect, due to errors in the internal optics.The greatest challenge in the direct detection of Earth-like planets is the development of precision wavefront correction. It is conceptually useful to divide the various internal error/noise sources into two categories: statistical and systematic. It is beyond the scope of this paper to describe all the error and noise sources in detail, nevertheless, their main sources and their impact on the design are summarized here. The random arrival of photons is considered a statistical noise source. Other statistical errors are caused by diffracted background light, local and exo-zodi*, stray light, and detector read noise. Systematic errors arise from wavefront phase and amplitude errors, scattered light, polarization, chromatic effects, and pointing error.

While there are many sources of error in the system, the most significant is wavefront distortion (also known as "aberrations") due to imperfect optics. Traditionally, these imperfections are divided into phase and amplitude aberrations. Phase aberrations are caused by optical surface height variations, while amplitude aberrations are caused by reflectivity variations across the surfaces as well as polarization effects. These aberrations can scatter light in the image where discovery takes place, at intensities several orders of magnitude larger than the planet light. Wavefront accuracy on the order of $\lambda/10,000$ is necessary in order to achieve the desired contrast for Earth-like planets imaging. Current optical components polishing technology can achieve accuracy between $\lambda/100$ and $\lambda/500$, depending on the size of the component. Therefore, a visible light TPF must be equipped with an active wavefront control system. Currently, all proposed solutions to the space-based high contrast imaging problem address the contrast issue in its ideal form with no aberrations in the system.[10,19,21] However, the correction algorithms lag behind.

While the wavefront control system can, in theory, correct any static, monochromatic wave front over a useful range of spatial frequencies, the system is limited in its broad band performance. This is because the aberrations, reflectivity variations, and propagations in the optical train have wavelength dependencies that are not necessarily matched to the wavelength dependence of the wavefront control system. Consider for example a metal-coated mirror located somewhere between the image plane and pupil plane. If the mirror coating has gray blemishes, they propagate to the pupil and generate phase errors that are proportional to wavelength.[26] A DM in the pupil compensates the phase by adjusting the surface height, and the phase varies as $1/\lambda$. Thus, ideal correction is achieved at just the central (or other appropriate) wavelength. Shaklan and Green[26] compared two wave front control configurations, a zero path length difference Michelson interferometer and sequential arrangement of the DMs, and showed that the sequential configuration provides superior broad-band performance while relaxing the aberration and reflectivity uniformity requirements throughout the system. The sequential configuration relies on propagation of aberrations introduced at a non-pupil conjugate DM to create wavelength-independent amplitude at the system pupil.

*zodiacal light is diffracted light from various small dust particles in the planetary system.

Give'on showed that the frequency folded light generated by mixing of high-spatial frequencies beyond the control bandwidth of the DM creates a $1/\lambda^2$ amplitude dependence in the pupil.[28] Shaklan, Green, and Palacios[29] then showed that the scattered light arising from frequency folding on an existing large optic (the 8 m diameter VLT) was within the TPF-C requirements. Thus this broad-band term does not need to be corrected if the TPF-C primary is constructed to the same tolerances as a VLT primary.[30]

4. WAVEFRONT CORRECTION

TPF-C assumes a "set and forget" approach to wavefront control. In this approach, the wave front is controlled once at the beginning of an observation, and is required to remain stable for the duration T of the observation. This approach places demanding requirements on the system since observations can be long ($\sim$ 1 day) and stability requirements are extremely challenging, as will be shown below. However, a set-and-forget approach is straightforward to model and clear engineering requirements for well-defined periods can be defined. The requirements are not blurred by various control bandwidths, and they are not relaxed by as-yet unproven high-dynamic range wavefront control. In the future, once detailed end-to-end models of active wavefront control demonstrate the ability to reduce speckles to a level of 1×10^{-10} and estimate their value to 2×10^{-11}, we will consider changing to an active approach and subsequently relaxing temporal stability requirements.

Time is of the essence in this mission. Integration times are long and the duration of the mission may be limited to a few years. The time spent setting the wave front should be small compared to the time spent integrating on planet light. This is not yet the case for the current speckle nulling algorithm.[17] In this section we introduce a potentially more efficient approach, the 'peek-a-boo' algorithm.

The "Peak-a-boo" correction method is a closed loop correction algorithm that iteratively finds the shape of the DM that minimizes the total intensity of light in a predetermined region on one side of the image plane. Each iteration consists of two stages, a reconstruction stage and a correction stage. In the reconstruction stage, the complex valued electric field at the image plane is reconstructed from a set of three intensity measurements of the electric field. In the correction stage, the DM is updated based on the information acquired in the reconstruction stage.[30] This algorithm is described in more detail in a separate paper.[18]

Consider the shaped pupil coronagraph. Let Φ be the difference between the effective aberration and unity in the pupil plane,

$$\Phi(x,y) = e^{\alpha(x,y)+i\frac{2\pi}{\lambda}\beta(x,y)} - 1, \tag{1}$$

where x and y are the pupil plane coordinates, λ is the wavelength of light, and α and $\frac{2\pi}{\lambda}\beta$ are the amplitude and phase aberrations in the system, respectively. Assuming a superposition model for the $N_{DM} \times N_{DM}$ actuator DM, with a known influence function, f, scaled by an actuator height, a, the condition for minimum energy in a given region, $\mathcal{H}$, on one side of the image plane is that for all $k, l \in [1, N_{DM}]$,

$$\sum_{m=1}^{N_{dm}} \sum_{n=1}^{N_{dm}} a_{m,n} \Re\left\{\left\langle \widehat{Af}_{m,n}(\xi,\eta), \widehat{Af}_{k,l}(\xi,\eta)\right\rangle\right\} = \frac{\lambda}{2\pi} \Im\left\{\left\langle \widehat{A\Phi}(\xi,\eta), \widehat{Af}_{k,l}(\xi,\eta)\right\rangle\right\}, \tag{2}$$

where ξ and η are the image plane coordinates, λ is the wavelength, A is the shaped pupil function, the hat operator represents the Fourier transform, and the inner product is defined as

$$\langle f, g\rangle = \int\int_{\mathcal{H}} f^*(\xi,\eta) g(\xi,\eta) \mathrm{d}\xi \mathrm{d}\eta. \tag{3}$$

In order to reconstruct $\widehat{A\Phi}(\xi,\eta)$, a pinhole is added at the center of the shaped pupil. Three images are recorded. The first with the pinhole blocked, $I_1(\xi,\eta)$, the second with the pinhole open, $I_2(\xi,\eta)$, and the third, with the pinhole open and a quarter wave plate across the pinhole (or equivalently actuating the DM element conjugate to the pinhole by 1/8 wave), $I_3(\xi,\eta)$. Then,

$$\widehat{A\Phi}(\xi,\eta) = \frac{I_2(\xi,\eta) - I_1(\xi,\eta) - \widehat{h}^2(\xi,\eta) + i\left[I_3(\xi,\eta) - I_1(\xi,\eta) - \widehat{h}^2(\xi,\eta)\right]}{2\widehat{h}(\xi,\eta)}, \tag{4}$$

where $\widehat{h}(\xi,\eta)$ is the Fourier transform of the pinhole function, $h(x,y)$.

The following shows simulations of the "Peak-a-boo" algorithm with the shaped pupil coronagraph. Figure 2 shows the pupil function (left) and its ideal PSF (center) that were used in this section. The right image in figure 2 shows the PSF with phase and amplitude aberrations included. The phase aberration was simulated with $RMS = \lambda/200$ and a $\nu^{-3/2}$ power law. The amplitude aberration was simulated with $RMS = 0.005$ and a ν^{-2} power law.

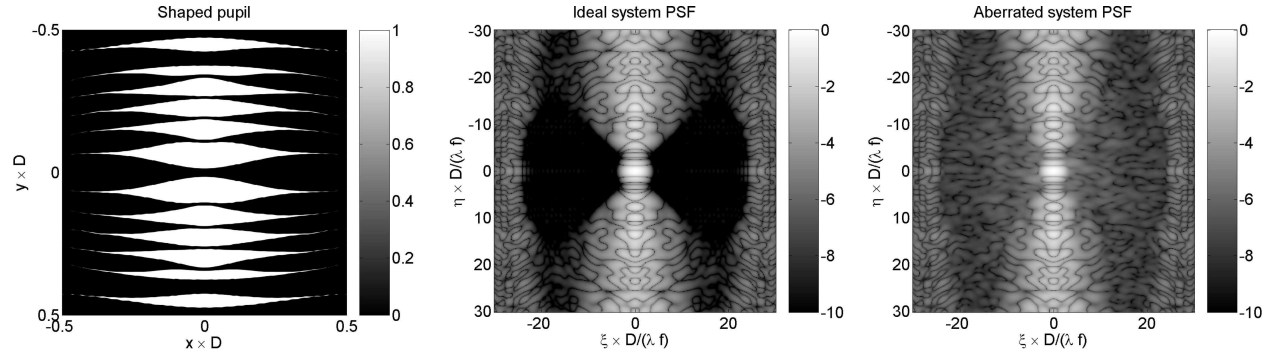

Figure 2. The ideal and aberrated system PSF. Left: The pupil function used in all the simulations in this section (linear scale). Center: The PSF of the ideal system (log scale). Right: The PSF of the aberrated system using the amplitude and phase aberrations described above (log scale). In order to compare different settings and different systems, those are the aberrations used throughout the section.

A circular pinhole, 1 millimeter in diameter, was added in the center of the shaped pupil. A DM was simulated with 32×32 actuators, evenly spaced on a square grid and the dark region was defined as $\mathcal{H} = \{\xi,\eta \mid 4\frac{\lambda f}{D} \le \xi \le 15\frac{\lambda f}{D}, -15\frac{\lambda f}{D} \le \eta \le 15\frac{\lambda f}{D}\}$. Figure 3 shows on the left the PSF of the corrected system after 4 iterations and a log plot of the average intensity in the dark zone per iteration on the right. The average intensity per iteration is compared to the average intensity for a system without aberrations.

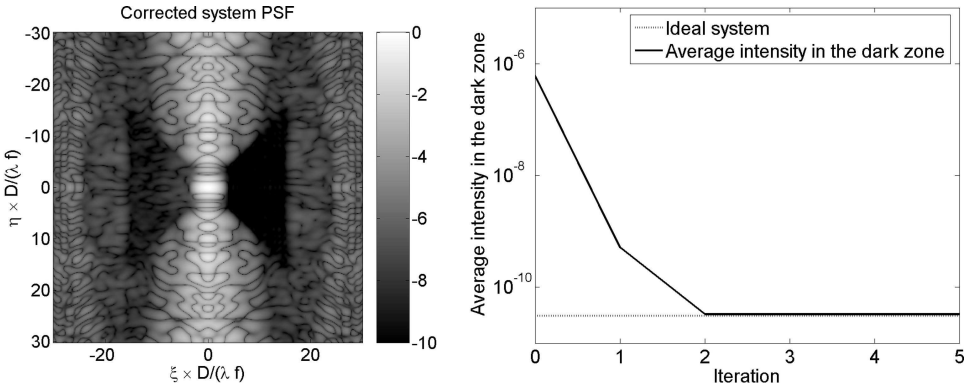

Figure 3. Simulation results for the ideal case. Left: The PSF of the corrected system after the correction algorithm converged (log scale). Right: A plot of the average intensity of the corrected PSF in the dark zone per iteration compared to the system without aberrations.

As seen in figure 3, the corrected system converges after 3 iterations to the nominal intensity in the dark zone.

The "Peak-a-boo" algorithm has also shown promise with broadband light. Without any modifications to the algorithm itself, figure 4 shows the effect of applying it to a system with wavelength band of $\lambda/\Delta\lambda = 10$.

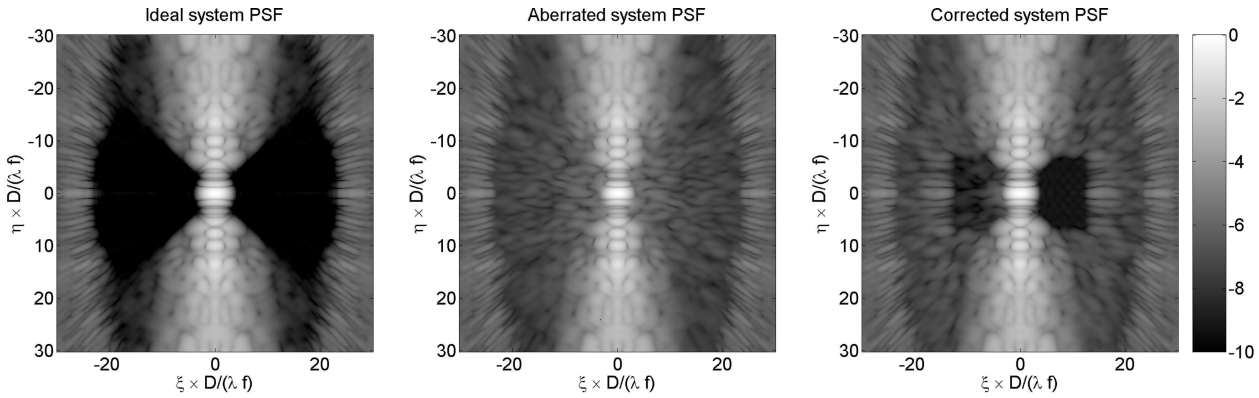

Figure 4. Simulation results for a system in $\lambda/\Delta\lambda = 10$ wavelength band. Left: The nominal system. Center: The system with amplitude and phase aberrations. Right: The corrected system after 4 iterations of the "Peak-a-boo" algorithm.

As seen in figure 4, the correction system converges to a contrast of 10^{-9}, which is consistent with the expected effect of using broadband light with one DM.[26]

5. SUMMARY

There has been tremendous progress in the field of high contrast imaging in the past few years, both in innovative designs and correction algorithms. Originally, the most promising design was the Lyot coronagraph and the only correction method was the speckle nulling. Since then, many designs have been proposed and investigated, some are related in design to the Lyot coronagraph (e.g. band limited Lyot coronagraph and the OVC) and some are very different (e.g. SPC and PIAA). High-contrast test facilities around the world are studying these approaches and pushing the technology toward the required 10^{10} contrast level.

On the other hand, there has not been as much progress in correction algorithms. As of today, the only tested algorithm is the speckle nulling at HCIT. It is our belief that, in its present form, this algorithm is not suitable for TPF due to the number of iterations needed to achieve the desired contrast. We presented an innovative correction method for the SPC, the "Peak-a-boo", which relies on image plane measurements with the addition of a pinhole to the shaped pupil. We are currently investigating how to incorporate the "Peak-a-boo" algorithm into the Lyot coronagraph by adding the pinhole to the Lyot stop. In simulations the "Peak-a-boo" has shown far better performance than the speckle nulling with respect to iterations needed to reach 10^{10} contrast. In addition, this algorithm has shown promise in broadband light.

A portion of this work was carried out at the Jet Propulsion Laboratory, California Institute of Technology, under contract with the National Aeronautics and Space Administration.

REFERENCES

1. Ford, V.G., et al, *The Terrestrial Planet Finder Coronagraph 2005: Overview of System Design Studies and Technology Development*, Proc. SPIE Vol. 5905 (2005).
2. Brown, R.A., *Single Visit Photometric and Obscurational Completeness*, The Astrophysical Journal, 624, pp. 1010-1024 (2005).
3. Ford E. B., Seager S., and Turner E. L. *Characterization of extrasolar terrestrial planets from diurnal photometric variability.* Nature, 412(885), 2001.
4. Seager S., Turner E. L., Schafer J., and E. B. Ford., *Vegetations red edge: A possible spectroscopic biomarker of extraterrestrial plants.* Astrobiology, 5(372), 2005.
5. Beichman C.A., Woolf N.J., and Lindensmith C.A. *The Terrestrial Planet Finder*, volume 99-3. Pasadena: JPL Publication, 1999.
6. Des Marais D. J., Harwit M., Jucks K., Kasting J., Lin D., Lunine J., Schneider J., Seager S., Traub W., and Woolf N., *Remote sensing of planetary properties and biosignatures on extrasolar terrestrial planets.* Astrobiology, 2(2):153–181, June 2002.
7. Traub, W.A. and Jucks K.W., *A possible aeronomy of extrasolar planets* in Atmospheres in the Solar System: Comparative Aeronomy, edited by Mendilo M., Nagy A. and Waite H.J., AGU Geophysical Monograph. 130, 369-380, 2002.
8. Kasdin N.J., Brown R.A., Burrows C.J., Kilston S., Kuchner M., Littman M.G., Noecker M.C., Seager S., Spergel D.N., Turner E.L., Traub W.A., Vanderbei R.J., and Woodruff R.A. *An optical/uv space coronagraph concept for the terrestrial planet finder.* Advances in Space Research, 34:625–630, 2004.
9. Lyot B., MNRAS, 99:580, 1939.
10. Kuchner M.J. and Traub W.A. *A coronagraph with band-limited mask for finding terrestrial planets.* The Astrophysical Journal, 570:900+, 2002.
11. Kuchner M.J. and Spergel D.N. *Notch filter masks: Practical image masks for planet-finding coronagraphs.* The Astrophysical Journal, 594:617–626, 2003.
12. G. Foo, D. M. Palacios, and G. A. Swartzlander, Jr., *Optical vortex coronagraph,* Optics Letters 30, 3308-3310 (2005)
13. Rouan D., Riaud P., Boccaletti A., Clenet Y., Labeyrie A., *The Four-Quadrant Phase-Mask Coronagraph. I. Principle* Publication of the Astronomical Society of the Pacific, 112: 1479-1486, 2000 November
14. Palacios D. M., *An optical vortex coronagraph*, Proceedings of SPIE, Volume 5905, 2005.
15. Schwartzlander, G. A., *Achromatic optical vortex lens,* Opt. Lett., 31, 2042-2044 (2006).
16. Shaklan S. B., Green J. J., *Low-Order Aberration Sensitivity of Eighth-Order Coronagraph Masks* The Astrophysical Journal, 628:474-477, July 20, 2005.
17. Trauger J. T. , Burrows C. , Gordon B. , et al, *Coronagraph contrast demonstration with the high-contrast imagaing testbed,* Proc. SPIE 5487 1330-1336 (2004).
18. Give'on A., Kasdin N.J., Vanderbei R.J., *Closed-loop wavefront correction for high-contrast imaging: the "peak-a-boo" algorithm.*, Proc. SPIE 6306 (Aug 2006).
19. Guyon O., Pluzhnik E. A., Galicher R., Martinache F., Ridgway S. T., and Woodruff R. A., *Exoplanet imaging with a phase-induced amplitude apodization coronagraph. i. principle.* The Astrophysical Journal, 622:744-758, March 2005.
20. Pluzhnik E. A. et. al. *Exoplanet Imaging with Phase-Induced Amplitude Apodization Coronagraph. III. Diffraction Effects and Coronagraph Design*, The Astrophysical Journal, 644:12461257, 2006 June 20
21. Kasdin N.J., Vanderbei R.J., Spergel D.N., and Littman N.G., *Extrasolar planet finding via optimal apodized and shaped pupil coronagraphs.* The Astrophysical Journal, 582:1147–1161, January 2003.
22. Slepian D. *Analytic solution of two apodization problems.* Journal of the Optical Society of America, 55:1110–1115, 1965.
23. Slepian D. and Pollack H.O. *Prolate spheroidal wave functions, fourier analysis and uncertainty.* The Bell System Technical Journal, pages 43–84, January 1961.
24. Vanderbei R.J, Kasdin N.J, Spergel D.N., and Kuchner M., *New pupil masks for high-contrast imaging.* Proceedings of SPIE - Techniques and Instrumentation for Detection of Exoplanets, 5170:49–56, 2003.

25. Shaklan S. B., Green J. J., *Low-order aberration sensitivity of eighth-order coronagraph masks,* ApJ 628, 474-477 (2005).
26. Shaklan S. B., Green J. J., *Reflectivity and optical surface height requirements in a broadband coronagraph. 1.Contrast floor due to controllable spatial frequencies,* Appl. Opt. 45, 5143-5153 (2006)
27. Littman M.G. et. al., *Phase and Amplitude Control Ability using Spatial Light Modulators and Zero Path Length Difference Michelson Interferometer*, Proc. SPIE Vol. 4854, Feb 2003
28. Give'on A., Kasdin N. J., Vanderbei R. J., Avitzour Y., *On representing and correcting wavefront errors in high-contrast imaging systems,* The Journal of the Optical Society of America A, Vol. 23, pp. 1063-1073, May 2006.
29. Shaklan S. B., Green J. J., Palacios D.M. *The Terrestrial Planet Finder Coronagraph optical surface requirements*, Proc. SPIE Vol. 6265, Jul 2006.
30. Borde P. J. and Traub W. A., *High-contrast imaging from space: Speckle nulling in a low aberration regime.* Applied Physics Journal, 638, February 2006.